PLP-Dependent Enzyme Methionine γ-Lyase: Insights into the Michaelis Complex from Molecular Dynamics and Free Energy Simulations

Xingyu Chen, Nathan Ferchaud, Pierre Briozzo, David Machover, Thomas Simonson

The PLP-dependent enzyme methionine gamma-lyase: insights into the Michaelis complex from molecular dynamics and free energy simulations

Xingyu Chen,[†] Nathan Ferchaud,[‡] Pierre Briozzo,[‡] David Machover,[¶] and Thomas Simonson[*,†]

†*Laboratoire de Biologie Structurale de la Cellule (CNRS UMR7654), Ecole Polytechnique, Palaiseau, France*

‡*Institut Jean-Pierre Bourgin, INRAE-AgroParisTech, University Paris-Saclay, Versailles, France*

¶*INSERM U935-UA09, University Paris-Saclay, Hôpital Paul-Brousse, 12, Avenue Paul Vaillant-Couturier, 94800 Villejuif, France*

E-mail: thomas.simonson@polytechnique.fr

Abstract

Methionine gamma-lyase (MGL) breaks down methionine, with the help of its cofactor pyridoxal-5'-phosphate (PLP), or vitamin B6. Methionine depletion is damaging for cancer cells but not normal cells, so that MGL is of interest as a therapeutic protein. To increase our understanding and help engineer improved activity, we focused on the reactive, Michaelis complex $\mathcal{M}$ between MGL, covalently-bound PLP, and substrate Met. $\mathcal{M}$ is not amenable to crystallography, as it proceeds to products. Experimental activity measurements helped exclude a mechanism that would bypass $\mathcal{M}$. We then used molecular dynamics and alchemical free energy simulations to elucidate its structure and dynamics. We showed that the PLP phosphate has a pK_a strongly downshifted by the protein, whether or not Met is present. Met binding affects the structure surrounding the reactive atoms. With Met, the Schiff base linkage between PLP and a nearby lysine shifts from a zwitterionic, keto form to a neutral, enol form that makes it easier for Met to approach its labile, target atom. The Met ligand also stabilizes the correct orientation of the Schiff base, more strongly than in simulations without Met, and in agreement with structures in the Protein Data Bank, where the Schiff base orientation correlates with the presence or absence of a co-bound anion or substrate analog in the active site. Overall, the Met ligand helps organize the active site for the enzyme reaction by reducing fluctuations and shifting protonation states and conformational populations.

Keywords: enzyme mechanism, vitamin B6, molecular mechanics, protein structure

Introduction

Methionine gamma-lyase, or MGL, breaks methionine down into α-ketobutyrate, ammonia and methane thiol.[1] It depends on the cofactor pyridoxal-5'-phosphate, or PLP, which is the catalytically-active form of vitamin B6 and participates in over 160 enzyme reactions.[2–4] MGLs are found in bacteria, protozoa and plants, but not mammals. Cancer cells cannot survive methionine deprivation,[5] whereas normal cells are more resistant. Therefore, MGL has been proposed as an anticancer tool that can digest methionine and reduce the growth of cancer cells.[5] For therapeutic applications, specific bacterial MGLs may need to be modified by protein engineering,[5,6] to optimize stability, activity, specificity or immunogenicity. For example, the enzyme from *Brevibacterium aurantiacum* is a strong candidate, since it is present in food and should have low immunogenicity.[5,7] However, its activity decreases in serum too rapidly for therapeutic use, for reasons that are not fully understood. Understanding is essential to guide engineering efforts, and molecular modeling is a powerful tool to help provide it. In particular, functional states that are transient and inaccessible to X-ray crystallography can be readily characterized through simulations. This includes the pre-catalysis, Michaelis complex, considered in this work.

The main states involved in the MGL reaction are schematized in Fig. 1. Both methionine (Met) and PLP must bind, and PLP must become covalently attached to an active site Lys through a Schiff base linkage (Fig. 1A). The reactive, Michaelis complex $\mathcal{M}$ = Met:MGL-PLP is then in place, where "-" denotes covalent linkage. In addition to $\mathcal{M}$, four intermediate states can be populated (Fig. 1B). From $\mathcal{M}$, the reaction can proceed: Met reacts with PLP at the C4' atom, forming a tetrahedral intermediate, and displacing Lys to form an external aldimine with PLP. Met is then cleaved at the γ-position and

methane thiol is eliminated. Finally, the remaining, α-keto acid is released from PLP along with ammonia, and these dissociate.[1]

All these reaction steps and intermediates can potentially be engineered, a daunting set of possibilities. Fortunately, some simplifications can be made. In Fig. 1B, we have already excluded the possibility the reaction will proceed to products directly from the non-covalent Met:MGL:PLP complex. Indeed, MGL activity in the absence of the covalent PLP linkage is expected to be weak, as in related PLP enzymes.[8,9] We confirm this experimentally in this work, by comparing turnover numbers of wildtype MGL to two mutants that are unable to bind PLP covalently; see Results. We can also assume the binding steps are fast compared to those that make or break covalent bonds. The states within the two boxes (Fig. 1B) are then at equilibrium, and a stationary state is rapidly reached for the righthand box, as in Michaelis-Menten theory. The fluxes in and out of the box are then equal. If we make the stronger assumption that the covalent steps are irreversible, the overall reaction rate takes the simple form:

$$\mathrm{d[products]/dt} = k_{\mathrm{cat}}\ [\mathrm{Met{:}MGL\text{-}PLP}] = k_P\ [\mathrm{MGL{:}PLP}] + k'_P\ [\mathrm{Met{:}MGL{:}PLP}],$$

where k_{cat}, k_P, k'_P are rate constants (Fig. 1B), MGL:PLP and Met:MGL:PLP are the non-covalent complexes, and the righthand equality uses flux conservation. If we assume $k_P \approx k'_P$, the overall rate increases with [MGL:PLP] + [Met:MGL:PLP], the total concentration of non-covalently bound PLP. Thus, to speed up MGL, we should focus on improving non-covalent PLP binding.

Other questions remain. What are the structures, fluctuations, and populations of the intermediate states? How is the substrate Met positioned? Which PLP tautomers predominate? The PLP phosphate can be protonated or not, and the Schiff base linkage exhibits a keto-enol tautomerism.[10–12] Earlier, we studied the MGL-PLP complex.[13] We were able to characterize structural and dynamical properties that are not revealed by

the crystal structure and to determine the main PLP protonation states.[13] Here, we considered an additional functional intermediate: the reactive complex $\mathcal{M}$ of MGL-PLP with Met. In a future paper, we will consider the non-covalent MGL:PLP complex. $\mathcal{M}$ is the essential, pre-catalysis, Michaelis complex, while MGL:PLP is one of the two non-covalent complexes we would like to engineer for increased PLP binding. Both are inaccessible to X-ray crystallography, since $\mathcal{M}$ will spontaneously proceed to products, while MGL:PLP will become covalently linked over time. Thus, modeling these states fills an important gap.

We considered the enzyme from *Pseudomonas putida*,[1,5] which has been extensively studied in view of cancer treatments. We refer to it below as ppMGL. We first measured turnover numbers experimentally for wildtype and two mutants that cannot form a covalent linkage to PLP, showing that their activity is very low. This indicates that the reaction cannot proceed directly from Met:MGL:PLP and must first proceed to the Michaelis complex $\mathcal{M}$. We then used alchemical free energy perturbation simulations (FEP) to determine the preferred PLP protonation states in the presence of the Met substrate (Met:MGL-PLP, referred to as the holo protein) and in its absence (MGL-PLP, referred to as the apo protein). We distinguish four states, which have a -1 or -2 phosphate charge, and a neutral or zwitterionic tautomer for the Schiff linkage; we refer to them as N1 (neutral, -1 charge), N2, Z1, Z2 (zwitterionic, -2 charge); see Fig. 2A. We also performed a statistical analysis of MGL structures in the PDB, which reveal the effect of co-bound ions and substrate analogs on the binding pocket conformation. We used molecular dynamics (MD) to characterize the interactions formed by Met within the binding pocket, and the subtle changes that occur in the pocket when Met is introduced. We distinguish in particular two orientations for the Schiff base linkage: an "A" orientation with the linking NZ atom pointing towards an anion binding site, and a "B" orientation

where it points backwards, into the binding pocket; see Fig. 2B. The following section describes the computational methods employed. We give the formalism to compute the pK_a of the PLP phosphate, followed by the FEP methodology and the MD simulation details. Results are described next. The FEP simulations showed that the phosphate pK_a is not strongly altered by Met binding, but the keto/enol equilibrium shifts towards the N2, keto form, which promotes conformations that are better suited for Met to react with PLP.

Materials and methods

The PLP phosphate pK_a: multi-tautomer formalism

Standard free energies and pK_a To compute the pK_a of the PLP phosphate, we take into account the existence of multiple tautomers for both the protonated and deprotonated states: N1/Z1 and N2/Z2, respectively (Fig. 2A). The pK_a shift between PLP in the protein complex and solution is given by:

$$pK_a^{\mathrm{prot}} - pK_a^{\mathrm{sol}} = \frac{1}{2.303kT}(\Delta G_P - \Delta G_S), \tag{1}$$

where k is Boltzmann's constant, T the temperature, and ΔG_P and ΔG_S are the standard PLP deprotonation free energies in the protein and solution. The experimental pK_a in solution is $pK_a^{\mathrm{sol}} = 6.3$,[14] while the difference between deprotonation free energies will be obtained from alchemical free energy perturbation simulations (FEP; see below). We introduce the free energies of the individual PLP tautomers, denoted $G_P(N1)$, $G_S(N1)$, and so on, where the subscript designates PLP in the protein (apo or holo) or solution. The differences between states are denoted $G_P(Z1) - G_P(N1) = \Delta G_P(N1 \rightarrow Z1)$, and so

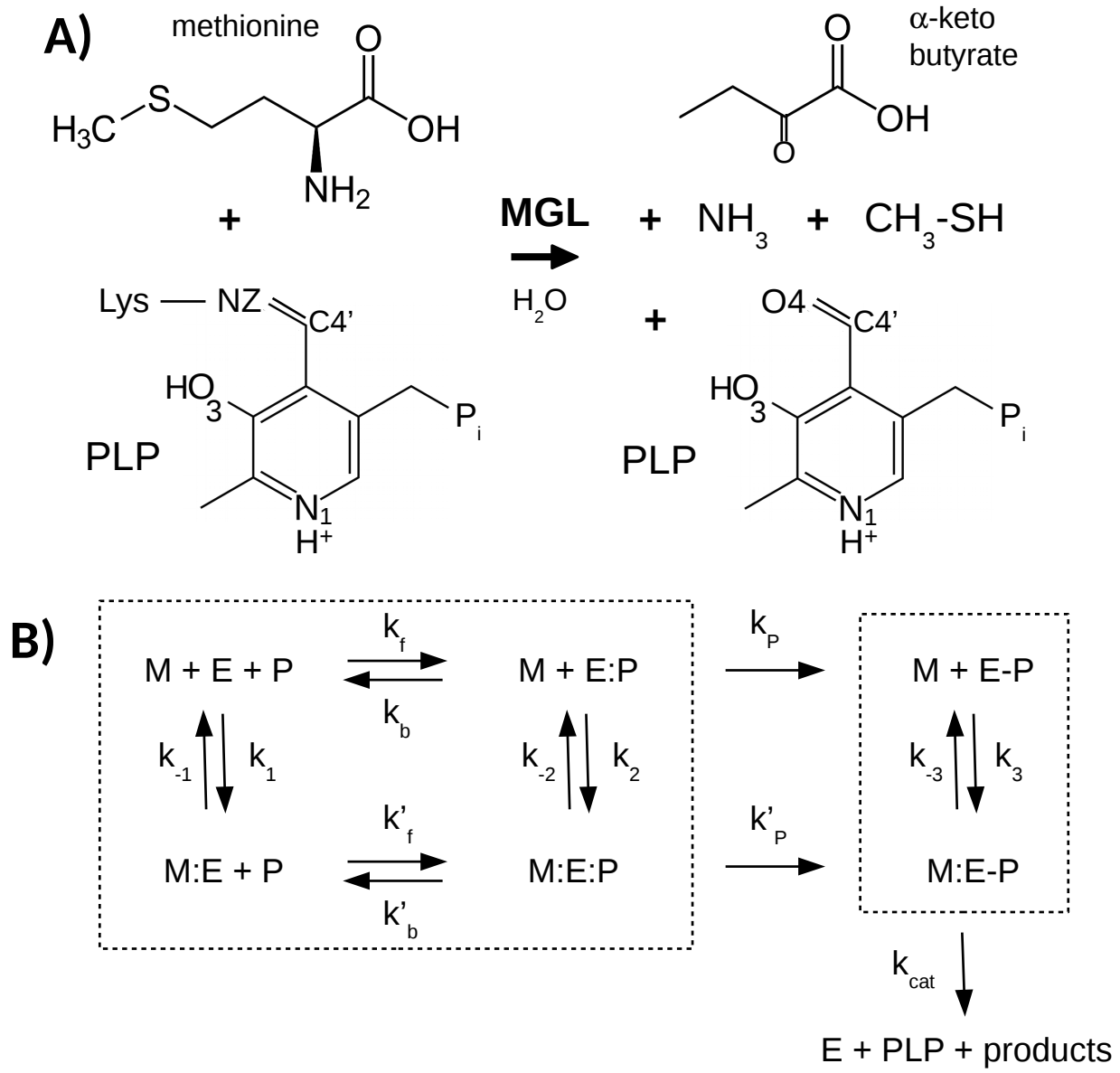

Figure 1: **MGL reaction. A)** Met reacts with the PLP cofactor to form products. **B)** Schematic of the reaction steps. M, E, P designate Met, enzyme, and PLP, respectively. Binding/unbinding reactions are grouped in dashed boxes. PLP bound to enzyme with and without a covalent linkage is denoted E:P and E-P, respectively. Rate constants for individual reaction steps are indicated beside each step.

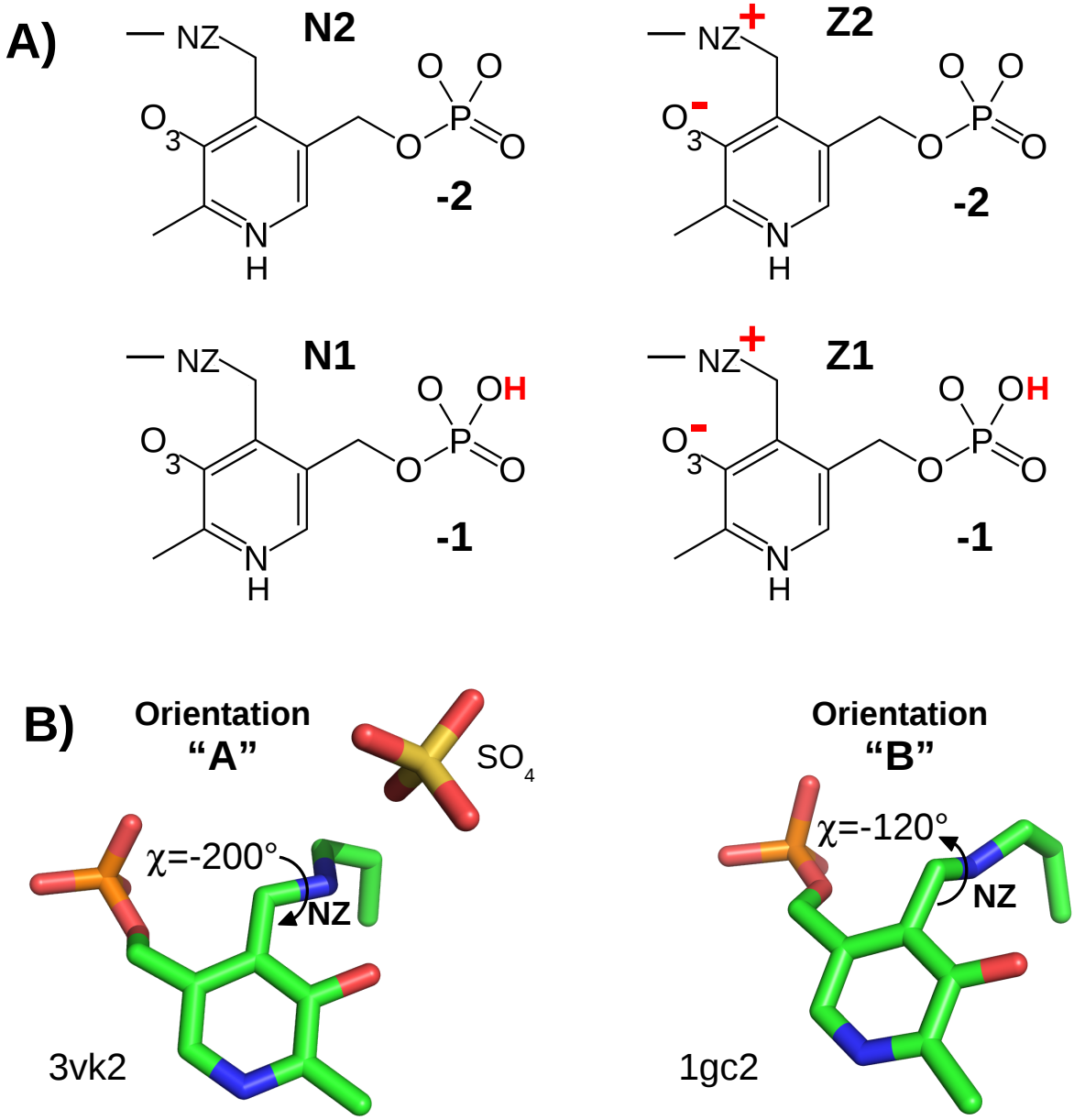

Figure 2: **PLP protonation states and conformers. A)** PLP protonation states. **B)** Two orientations "A" and "B" for the Schiff base linkage, represented by PDB entries 3vk2 (left) and 1gc2 (right), and characterized by the χ = CE-NZ-C4'-C4 torsion angle. 3vk2 contains a co-bound sulfate anion, shown here.

on. We do not assume a particular standard state; the relations below are general. The free energy change ΔG_P involves a Boltzmann average over tautomers:

$$e^{-\Delta G_P/kT} = \frac{e^{-G_P(N2)/kT} + e^{-G_P(Z2)/kT}}{e^{-G_P(N1)/kT} + e^{-G_P(Z1)/kT}} = e^{-\Delta G_p(N)} \frac{1 + e^{-\Delta G_P(N2 \to Z2)/kT}}{1 + e^{-\Delta G_P(N1 \to Z1)/kT}} \tag{2}$$

$\Delta G_P(N)$ is shorthand for $\Delta G_P(N1 \to N2)$, the N1 deprotonation free energy. Thus,

$$\Delta G_P = \Delta G_P(N) + \Delta G_P^{\rm conf}(N) = \Delta G_P(Z) + \Delta G_P^{\rm conf}(Z) \tag{3}$$

where $\Delta G_P^{\rm conf}(N)$, $\Delta G_P^{\rm conf}(Z)$ are corrections that are pH-independent and arise from the existence of multiple tautomers for each phosphate protonation state:

$$\Delta G_P^{\rm conf}(N) = -kT \ln \frac{1 + e^{-\Delta G_P(N2 \to Z2)/kT}}{1 + e^{-\Delta G_P(N1 \to Z1)/kT}} \tag{4}$$

and similarly for $\Delta G_P^{\rm conf}(Z)$ (swapping N and Z). For PLP in solution, we have the same relations, replacing all the subscripts "P" by "S". The formalism is readily extended to cases with more than two tautomers. $\Delta G_P^{\rm conf}(N)$ obeys some obvious limits. For example, if the tautomers have the same free energy, both $\Delta G_P^{\rm conf}(N)$ and $\Delta G_P^{\rm conf}(Z)$ reduce to $-kT \ln \frac{n_2}{n_1}$, where n_2, n_1 are the deprotonated and protonated tautomer numbers: a purely entropic contribution that favors the state with the most tautomers. If $\Delta G_P(N2 \to Z2)$ is large and negative while $\Delta G_P(N1 \to Z1)$ is large and positive, ΔG_P approaches $\Delta G_P(N1 \to Z2)$, as it should. If Z1, Z2 are much less (respectively, more) stable than N1, N2, $\Delta G_P^{\rm conf}(N)$ (respectively, $\Delta G_P^{\rm conf}(Z)$) is negligible.

Free energies and tautomer populations at neutral pH The phosphate deprotonation free energy in the protein is zero at pH = $pK_a^{\rm prot}$ and varies according to

$$\Delta G_P(pH) = -2.303\,kT\,(pH - pK_a^{\rm prot}) \tag{5}$$

and similarly for $\Delta G_S(pH)$. Since $\Delta G_P^{\rm conf}(N)$, $\Delta G_S^{\rm conf}(Z)$ are pH-independent, the pH-dependency of the deprotonation free energies $\Delta G_P(N1 \rightarrow N2)$, $\Delta G_S(N1 \rightarrow N2)$ follows:

$$\Delta G_P(N;pH) = -2.303\,kT\,(pH - pK_a^{\rm prot}) - \Delta G_P^{\rm conf}(N) \tag{6}$$

Since the N1/Z1 and N2/Z2 free energy differences are pH-independent, we obtain the relative free energies of all four states at any pH, from which the populations follow.

Free energy simulations of phosphate deprotonation

Modeling the N1 $\rightarrow$ N2 transformation The N1 $\rightarrow$ N2 transformation was studied earlier for MGL-PLP, in the absence of the Met ligand (apo protein). Here, we considered the protein in the presence of Met (holo protein). As before, the PLP phosphate was changed gradually from protonated to deprotonated over a series of MD simulations.[13] Because the proton has no van der Waals interactions in the force field employed, deprotonation could be modeled as a redistribution of atomic charges. We switched the partial charges of PLP from the N1 to the N2 state, in the protein or solution, through a series of 5 simulations, identified by a progress variable λ that varied from 0 to 1. Five values were simulated: $\lambda = 0$ (singly-protonated), 0.25, 0.5, 0.75, 1 (fully-deprotonated). 40–80 ns were run for each λ value. In each series (or "run"), the endpoint of the simulation at one λ value served as the starting point for the next value, e.g., $\lambda + 0.25$ in the forward

direction. Overall, we did two runs in the forward direction (λ values 0 and 0.25 only) and two complete runs in the backwards direction, totalling 160 ns of MD for each λ value, and 800 ns overall. The free energy changes for each λ interval were estimated both with the Bennett acceptance ratio method (BAR)[15] and with a thermodynamic integration method (TI).[16] For TI, the free energy derivative $\partial G/\partial\lambda$ at each λ value was obtained by a finite-difference approximation.[13] The derivatives were interpolated using cubic splines and integrated.

Extrapolating to the thermodynamic limit When MD is used to study a dilute protein solution, the finite simulation box introduces artefacts.[17,18] For an ionic transformation like N1 $\rightarrow$ N2, a neutralizing charge is introduced to maintain a neutral box. This is done through a uniform charge density, or gellium.[18] The mean potential throughout the box is constrained to be zero. The potential is shifted to achieve this. To compare the protein and solution systems, we should adjust the protein system so that far from the protein, in the bulk-like solvent region, the mean potential is the same as in the solution system—namely, zero.[13] To compute the potential throughout the box, we used the VMD plugin pmepot,[19] which uses a uniform cubic grid that spans the simulation box. Grid points more than 12 Å from any protein atom were considered to be in the bulk-solvent-like region. Averaging over grid points and MD snapshots, we obtained a mean electrostatic potential Φ. Upshifting it to zero added -1 $\times$ Φ to the deprotonation free energy. Other box size artefacts were shown earlier to be small.[13]

PLP keto/enol or N/Z comparison

Modeling the keto/enol transformation We used the FEP method to compare the neutral, enol PLP state to the zwitterionic, keto state: N1 vs. Z1 or N2 vs. Z2, either in

the protein—with or without its Met ligand, or in solution. Displacement of the Schiff base proton from the linking oxygen O3 to NZ was modeled as a redistribution of atomic charges. Similar to pK_a methodology above, quantum mechanical effects such as covalent bond breaking were not explicitly accounted for. Rather, the system of interest was compared to a reference system, for which an accurate value was available that includes the quantum effects. Above, the pK_a reference was a model compound in solution: we subtracted FEP for the protein and the model compound, then "added back" the model compound through its experimental pK_a value. Here, we used a *gas phase* reference system, as previously.[13] Indeed, the keto/enol transformation was studied earlier with quantum mechanics,[11] providing the N/Z energy difference (-0.4 kcal/mol). Here, the N/Z comparisons were done with molecular mechanics for a PLP analog in the gas phase; the value was subtracted from the protein value; the model compound was then added back in through its quantum mechanical value.

Alchemical free energy perturbation simulations For the N2 $\rightarrow$ Z2 transformation in the protein, we used five MD windows, with the same λ values as for N1/N2. We also did a calculation with two windows, corresponding to the endpoints of the transformation, $\lambda = 0$ (neutral) and $\lambda = 1$ (zwitterionic). Results were almost identical (see below). For the transformations in solution, we also used five windows. For the N1 $\rightarrow$ Z1 transformation in the protein, a lower accuracy is acceptable, since are N1/Z1 weakly-populated. Therefore, we used just the two endpoint windows. Total simulations lengths per window were 1200 ns (N2/Z2) or 900 ns (Z1/N1). For the gas phase, we used a single, minimized structure for each endpoint, giving N $\rightarrow$ Z free energy changes of -44.0 kcal/mol.[13]

Sampling the Schiff base orientations In the protein, the Schiff base linkage has two available orientations (Fig. 2): a "forward" orientation, where the NZ atom points

towards an anion binding site, denoted "A", and a "backwards" orientation, with NZ towards the PLP phosphate, denoted "B". For MD sampling, care was needed to ensure both orientations were accounted for. There was a difficulty for N1 $\rightarrow$ Z1 in the apo-protein (no Met ligand). In the N1 state, the two orientations had essentially equal populations over 1200 ns of MD (49 vs. 51 %). In the Z1 state, only the A orientation was visited. This makes it impossible to reliably compute the free energy derivative at the Z1 endpoint. Instead, we used FEP to obtain the free energy difference between Z1 and the "A-orientation" substate of N1, also referred to as N1A: the N1 protonation state, restricted to be in the A orientation. The free energy difference of N1 is then simply $kT \ln 2$ lower than that of N1A.

Molecular dynamics setup

For the protein, we used the Amber ff14SB protein force field[20] force field. For the PLP cofactor, molecular mechanics parameters were derived earlier.[13] Four protonation states were treated: the phosphate group was singly- or doubly-charged, and the NZ-O3 atom pair had a proton either on NZ (zwitterionic, keto form "Z") or O3 (neutral, enol form "N"). The forms are referred to as Z1, Z2, N1, and N2.

Simulation systems were prepared using Xplor,[21] starting from the ppMGL crystal structure (PDB code 3VK3), which is a homotetramer. Position 116 was mutated from His back to the native type Cys. Each model involved a protein tetramer, spherically truncated to eliminate parts far away from the active site. Truncation spheres were centered on the PLP in one specific active site and had radii of 34 Å. Each truncated tetramer was solvated by an octahedral TIP3P water box.[22] Water molecules having an oxygen less than 2.5 Å from any nonhydrogen protein atom were deleted. A few sodium ions were added, to neutralize the total protein charge. The box edge length was 92 Å.

MD simulations were done as previously,[13] using periodic boundary conditions with a truncated octahedral box and the Particle Mesh Ewald method for electrostatics.[23] A 12 Å cutoff was applied to van der Waals and real-space electrostatic interactions. Temperature was maintained at 295 K using Langevin dynamics for nonhydrogen atoms. A pressure of 1 bar was maintained by the Langevin piston Nose-Hoover method.[24,25] For the MD production, residues within 5 Å of the edge of the protein truncation sphere were restrained to their initial positions.

PDB structure analysis

As previously,[13] we analyzed 25 PDB structures that all contained the PLP cofactor, covalently bound to lysine (Lys211 in ppMGL): 11 of ppMGL and 14 of orthologs. Removing symmetry images within each MGL tetramer left 60 independent monomers. We included structures that had no ligand (other than PLP) and ones that had as ligands either a small anion (sulfate or chloride) or an amino acid analog including a backbone carboxylate. The list is in Supplementary Table SM1. Molecular graphics images were generated using PYMOL, version 1.8 (www.pymol.org).

Experimental procedures

Production and purification of the purified ppMGL enzymes

pET28b (+) plasmids (Millipore, Molsheim, France) containing either the wild-type ppMGL (NCBI Reference Sequence: WP_274096805.1) or its K211A or K211Q variants were ordered from GenScript (Rijswijk, Netherlands). The cloning was in frame with a sequence coding a 6xHis tag at the protein C-terminus. Plasmid constructs were used to transform *Escherichia coli* HMS 174 (DE3) competent cells (Novagen; Merck, Darm-

stadt, Germany). Cells were grown at 37°C in Luria-Bertani medium containing 100 μg/mL ampicillin until A(600nm) reached 0.8. Temperature was lowered to 18°C, then isopropyl-β-D-1-thiogalactopyranoside was added (final concentration 1 mM) and cells were grown overnight. They were harvested by centrifugation at 6,000 $\times$ g for 15 min and washed with NaCl 0.9% (w/v). Cell pellets were frozen and stored at -80°C.

All purification steps were performed at 4°C. Bacterial cell pellets were thawed and resuspended in buffer A (50 mM HEPES-NaOH pH 7.5, 100 mM NaCl, 0.5 mM mM tris(2-carboxyethyl)phosphine, 10 mM imidazole, 20 μM PLP) containing protease inhibitor (cOmplete Mini EDTA-free, Roche, Indianapolis, USA). Cells were lysed with a One Shot cell disruptor (Constant Systems Ltd, Daventry, UK) at a pressure of 1.96 kbar. Extract was spun at 12,000 x g for 10 min at 4°C. Enzymes were purified from the supernatant by immobilized metal affinity chromatography (IMAC) on a Nickel HisTrap HP column (Cytiva, Vélizy-Villacoublay, France) connected to a NGC Medium-Pressure Liquid Chromatography System (Bio-Rad laboratories, Marnes-La-Coquette, France) in buffer A. Unbound proteins were washed, and bound proteins were eluted with a linear gradient of 0–500 mM imidazole. Purified proteins were concentrated using an Amicon Ultra-15 device (Merck Millipore, Darmstadt, Germany) with a molecular weight cut-off of 10 kDa. Concentration of the purified enzyme was then measured at 280 nm. UV-Visible absorption spectra were recorded in quartz cuvettes using a UV-1800 Shimadzu spectrophotometer.

Activity assay

MGL activity was measured using a colorimetric assay.[26] Activity was determined at 37°C in 100 mM potassium phosphate buffer (pH 8.0) and in the presence of 200 μM PLP and 100 mM methionine. Each enzyme was diluted in buffer A to an appropriate concentration

and added to start the reaction. After incubating the reaction mixture for the right amount of time in a tube with a sealed cap, the enzymatic reaction was terminated by adding trichloroacetic acid (final concentration 5% p/v). The solution obtained was then incubated 40 min at 50°C with 0.02% p/v of 3-methyl-2-benzothiazolone hydrazone hydrochloride (MBTH) in 0.5 M sodium acetate buffer (pH 5.0). MBTH reacts with the α-ketobutyrate reaction product to generate a compound absorbing at 320 nm (ϵ =15,740 M^{-1} cm^{-1}). k_{cat} was obtained by dividing the maximum rate of α-ketobutyrate production by the enzyme tetramer concentration.

Results

The need for covalent PLP linkage

In MGL enzymes, the PLP cofactor is bound in an aldimine linkage to the ϵ-amino group of a lysine, namely K211 in ppMGL. Formation of the PLP–Lys covalent bond leads to the Michaelis complex considered in this work (Fig. 1B). To confirm the importance of this linkage, we expressed and purified the K211A and K211Q variants of the enzyme. The wildtype enzyme absorption spectrum displays a maximum at 422 nm (Supplementary Fig. SM1) characteristic of PLP covalently bound to a lysine. In the spectra obtained with K211 variants, this peak is shifted to shorter wavelengths (415–420 nm), which are distinct from the 388 nm maximum observed for free PLP in solution at neutral pH,[27] and indicate a PLP aldehyde bound to the enzyme. Comparable results have been published for other PLP enzymes where the PLP-binding lysine was mutated, for instance with cystalysin[9] and D-amino acid transaminase.[28] In the case of the K258H variant of aspartate aminotransferase,[29] a crystal structure revealed PLP present in the active site (PDB code 1AKA). The K211A and K211Q variants of ppMGL therefore appear capable

of binding PLP non-covalently. As shown in Table 1, the turnover numbers of both variants were three orders of magnitude lower than those of the wildtype. This confirms that the reaction is unlikely to proceed from the noncovalent Met:MGL:PLP complex, and must proceed first to the Michaelis complex, as postulated in Fig. 1B.

Table 1: MGL turnover with and without covalent PLP linkage

Enzyme	wildtype	K211A	K211Q
$k_{cat}(s^{-1}$	31.8(7)	0.032(4)	0.0140(3)

For the wildtype, activity was measured after 5 min using an enzyme concentration of 0.01 mg/mL. To get a measurable signal for the variants, enzyme concentration was increased to 0.2 mg/mL and reaction time to 18 h. Results are the mean of five experiments, with standard deviation in parentheses in significant digits. No activity was observed with boiled enzyme or in the absence of enzyme.

PLP protonation states with FEP

We began by determining the preferred PLP protonation states (Fig. 2) in the Michaelis complex Met:MGL-PLP, using alchemical free energy perturbation simulations (FEP). Earlier, we used FEP to compute relative stabilities in the MGL-PLP complex: N2 vs. N1 and N2 vs. Z2,[13] which have a -2 or -1 phosphate and a neutral or zwitterionic Schiff linkage, respectively. Here, we considered Met:MGL-PLP and the effect of adding Met. We compared all four PLP states: Z1, N1, N2, Z2, to give a full picture and obtain the PLP phosphate pK_a in the absence and presence of Met. Supplementary Table SM2 reports free energy derivatives for each alchemical transformation: Z1 $\rightarrow$ N1 $\rightarrow$ N2 $\rightarrow$ Z2, along with their uncertainties. Thanks to the long MD simulations employed, the uncertainties were fairly small, in the range 2–8 kcal/mol for the derivatives and 1–2 kcal/mol for their integrals. The largest uncertainties were for Z1 $\rightarrow$ N1 cases, due to

the low stability of these states and their complexes with Met. Since they are weakly populated (see below), precision here is less important.

Table 2 reports the free energy differences between states, obtained by integrating the derivatives. Table 3 reports the populations of the four states in solution and in the apo and holo protein. The apo protein stabilizes the deprotonated PLP phosphate, compared to solution, downshifting its pK_a by 2.1 units, from 6.3 in solution to 4.2. Adding Met has a small effect, giving the same pK_a within 0.5 units. However, in the presence of Met, the N2/Z2 distribution is notably changed. In the apo protein, Z2 is 1.3 kcal/mol lower than N2, giving populations of 10% N2 and 90% Z2 (the other states being negligibly populated; Table 3). When Met is added, N2 becomes favored by 0.5 kcal/mol, giving holo populations of 69% N2 and 30% Z2 (Table 3). We show below that in MD structures, the N2 state is better adapted for the reaction between Met and the C4' atom of the PLP Schiff base linkage. This is also expected from simple electrostatic considerations, since the positive Met ammonium will have difficulty approaching the NZ–C4' group when NZ is in its protonated, keto state Z2. Overall, the Met ligand increases the N2 population 7-fold, shifting the PLP protonation state in a way that favors its own reaction with PLP.

Table 2: Alchemical free energy simulations for PLP phosphate pK_a

system X:	solution	apo protein MGL-PLP	holo protein Met:MGL-PLP
$\Delta G_X(N1 \rightarrow Z1)$	-2.4	+2.6	+1.0
$\Delta G_X(N2 \rightarrow Z2)$	-2.4	-1.3[a]	+0.5
$\Delta G_X^{\mathrm{conf}}(N)$	0.0	-1.4	-0.1
$\Delta G_X(N)$	-80.5[a]	-81.2[a]	-82.0
ΔG_X	-80.5	-82.6	-82.1
ΔpK_a	0.0	-2.1[b]	-1.6[b]
$\Delta G_X(N; pH = 7)$	-1.0	-3.0	-2.6

Free energies (kcal/mol) from alchemical FEP simulations.
[a]From earlier work.[13] [b]Shift relative to PLP in solution.

Table 3: Relative populations (%) of the four PLP forms

PLP form	Z1	N1	N2	Z2
solution	9.92	0.17	0.03	89.87
without Met	0.00	0.06	9.94	90.00
with Met	0.01	0.85	69.40	29.74

From alchemical FEP simulations.

PDB structures with/without bound ions or Met analogs

We analyzed 25 PDB structures (Supplementary Table SM1), including 11 of ppMGL and 14 of orthologs. They contained 60 subunits not related by crystal symmetry and where PLP was covalently bound to Lys in a Schiff base linkage (K211 in ppMGL). 10 structures (22 subunits) had no ligand other than PLP (apo structures). 15 had a ligand co-bound in the active site. The ligands in our dataset were either a small anion (sulfate in 6 structures, chloride in one) or an amino acid analog (8 structures, 15 subunits) with a backbone carboxylate group positioned at the anion site. The Met:MGL-PLP complex itself is not represented in the PDB, since it is chemically unstable, with Met proceeding to products. Notice that four PDB entries are described as Met complexes (3aej, 3aem, 3aen, 3vk3) and *do* contain Met in the structural models. However, the electronic density in their active sites *does not* reveal a Met ligand, as expected; an example is in Fig. 3. The density more probably corresponds to α-keto butyrate, produced by the reaction of substrate Met, catalyzed by the C116H enzyme variant during the crystallization time.

The ligands within the binding site are shown in Fig. 4A. All the bound ionic groups occupy the same position in the binding site, between the Lys211 NZ atom and the R375 side chain. This is also the position that is occupied by the Met carboxylate in the MD simulations, below. Selected structural variables are shown in Fig. 4B. Residues from neighboring subunits are designated with an asterisk. With a co-bound anion or carboxylate, the loop containing Y59* and R61* is well-ordered and the Y59* and R61*

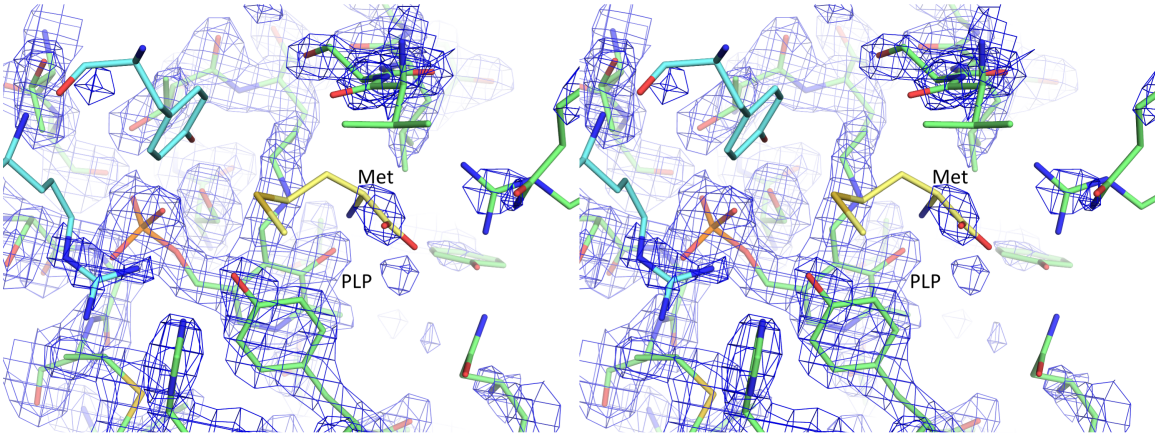

Figure 3: Structural model and electron density in the ppMGL active site from the 3VK3 PDB entry (subunit C). A 2 F_o - F_c map is shown, contoured at 2 standard deviations. Cross-eyed stereo view.

side chains interact closely with the PLP phosphate. Without such a ligand, these residues either have no visible electron density in the PDB models (15 of 22 subunits) or are much further from PLP. Half of the apo structures present a B orientation for the Schiff base NZ, pointing *backward* towards the PLP phosphate, as indicated by the NZ distances shown in Fig. 4B. In contrast, a co-bound anion or carboxylate always enforces the A orientation, with NZ pointing forward towards the *anion* site, as in Fig. 4A.

Structural comparison of the four PLP protonation states

Here, we describe MD simulations of MGL with all four PLP protonation states. The alchemical FEP simulations above showed that the dominant PLP states in Met:MGL-PLP are Z2 and especially N2 (Table 3). Nevertheless, it is of interest to apply MD to all four states and compare their structures, for two reasons. First, it reveals that while MD simulations of N2 and Z2 agree well with PDB structures, N1 and Z1 simulations agree poorly. This confirms the FEP results. Second, while N1 and Z1 are weakly populated, they might conceivably participate in the MGL reaction pathway. Therefore, we compare

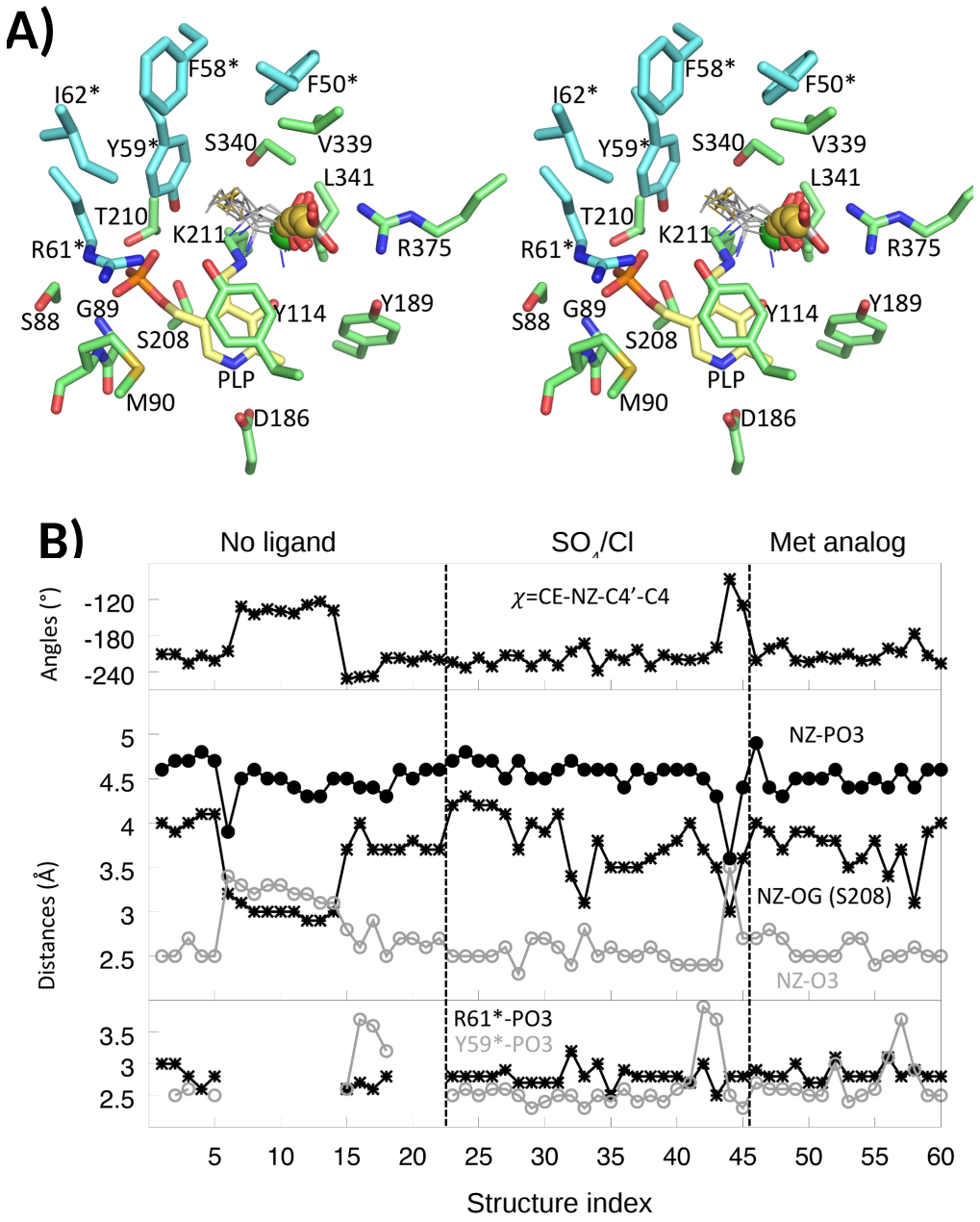

Figure 4: **A)** Small anions and substrate analogs bound in the active site of MGL. Cross-eyed stereo view. Met, PLP and selected side chains are shown as sticks. The small ionic ligands are indicated by spheres: chloride (green) and sulfate S atom (orange). The amino acid analogs are shown as thin lines, with sticks for their backbone carboxylates. **B)** Selected structural variables from PDB structures, with or without a co-bound ligand.

here the four states to each other and to the PDB, focussing on PLP and its surroundings. In the next section, we will focus on the substrate Met, its interactions, and its effect on the active site structure. RMS deviations of the active site structure did not drift over the MD simulations (with one exception), indicating stable MD structures, suitable for analysis. Selected structural variables from MD are shown in Fig. 5.

We consider first the PLP phosphate. It makes several interactions that depend strongly on its protonation state, as expected. During MD, a hydrogen bond with Y59* from the neighboring subunit is always formed with the N2 and Z2 states (-2 phosphate), but much less so with N1 (76% occupancy) and Z1 (52% occupancy). Comparison to the PDB is clear: all PDB structures with a co-bound anion or amino acid analog exhibit this hydrogen bond, except for two subunits (out of 38) where the interaction is a bit weaker. Thus, N2 and Z2 are consistent with the PDB data, while N1 and Z1 are not. The same situation is true for four other groups. The first is R61* from the neighboring subunit, whose salt bridge with the phosphate is present 100% of the time with N2 and Z2 but only 92% and 85% with N1 and Z1. Similar occupancies are seen for the M90 backbone amide, which hydrogen bonds to the phosphate strongly with N2 and Z2 and in the PDB, and more weakly with N1 and Z1, and for the side chains of S208 and T210. Finally, with N2, the phosphate forms a stable interaction with the Met ammonium, through a bridging water molecule. All these trends support N2 and Z2, while N1 and Z1 are not consistent with the PDB structures.

Another property that distinguishes N2/Z2 from N1/Z1 is the orientation of the Lys211 NZ and the Schiff base linkage, reflected by the dihedral angle NZ-C4'-C4-C5 and the distances of NZ from S208 and the PLP O3. N2 and Z2 agree well with the non-apo PDB structures, which all exhibit the A orientation (NZ towards the anion site), with one exception (out of 38 subunits), which has a co-bound chloride. In contrast, N1 and

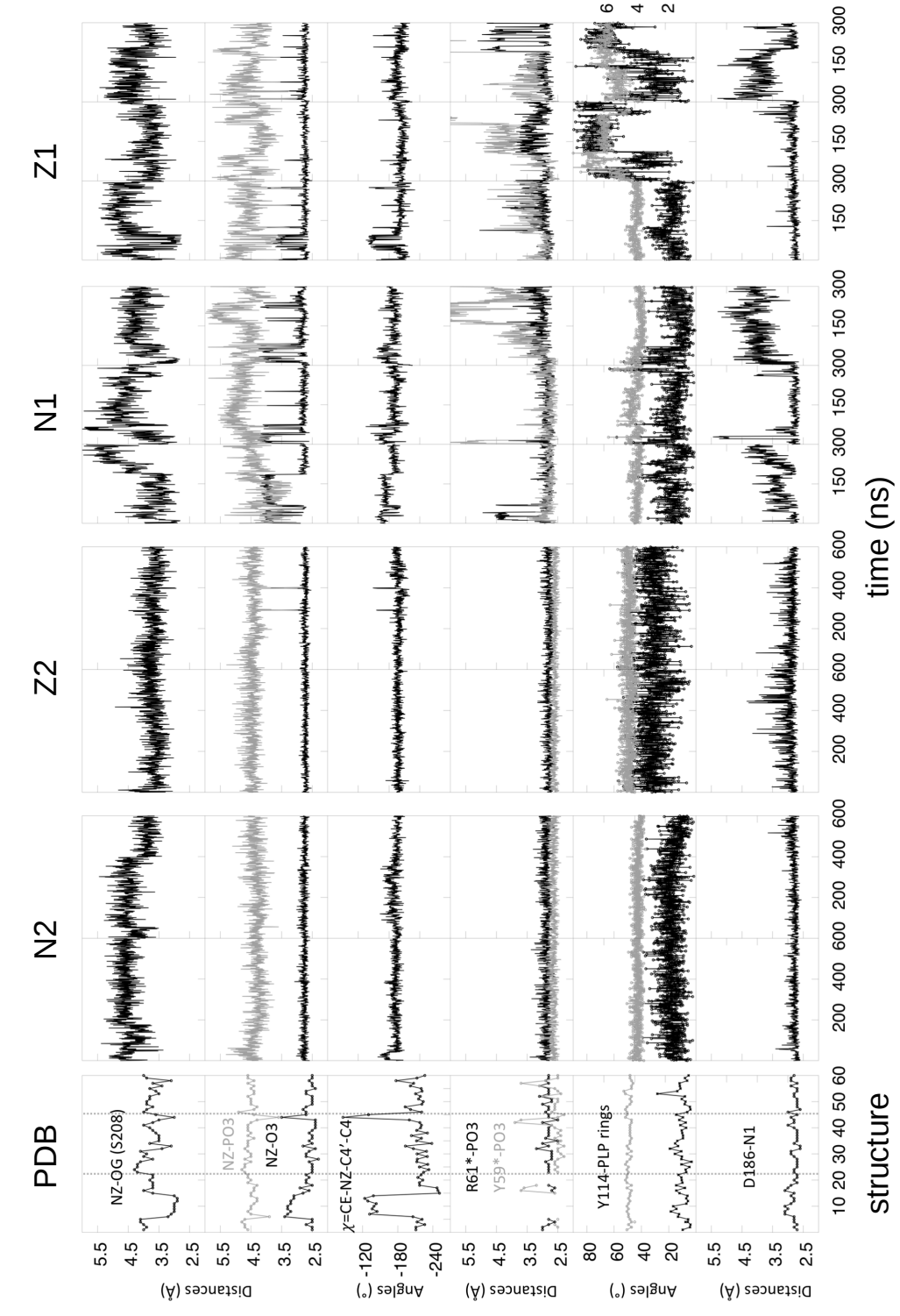

Figure 5: Time series of selected structural variables during MD.

especially Z1 fluctuate between the A and B orientations. For the NZ distance to the S208 OG atom, N2 yielded values slightly larger than the PDB (Table 4), while N1 and Z1 exhibited weaker interactions. For the NZ–O3 distance, N2, Z2 and Z1 agreed closely with the PDB (Table 4), whereas N1 exhibited larger values and fluctuations.

Table 4: Structural variables from PDB and MD

PLP form	PDB[a]	N2	Z2	Z1	N1
Lys211 NZ - O3 PLP	2.6(2)	2.8(1)	2.7(1)	3.2(6)	2.8(2)
Lys211 NZ - PO_3 PLP	4.5(2)	4.3(2)	4.5(2)	4.6(6)	4.5(5)
Lys211 NZ - S208	3.7(3)	4.4(4)	3.7(3)	4.2(7)	4.2(6)
Schiff orientation A[b]	97%[b]	100%	100%	67%	94%
PLP PO_3 - Y59*	2.6(4)	2.6(1)	2.6(1)	3.3(10)	4.2(17)
PLP PO_3 - R61*	2.8(1)	2.9(1)	2.8(1)	3.0(4)	3.1(5)
PLP PO_3 - N G89	2.8(1)	2.9(1)	2.9(1)	3.0(2)	3.0(2)
PLP PO_3 - N M90	2.9(1)	2.9(1)	2.8(1)	3.0(3)	3.0(4)
PLP PO_3 - S208	2.9(1)	2.8(2)	2.8(2)	3.0(6)	2.9(3)
PLP PO_3 - T210	2.7(1)	2.8(2)	2.7(1)	3.4(8)	3.2(7)
PLP N1 - D186	2.8(1)	2.8(1)	2.9(2)	3.4(6)	3.1(5)
PLP ring - Y114	4.4(1)	3.8(2)	4.4(3)	3.9(3)	5.3(15)
PLP ring - Y114[c]	10(5)	18(7)	31(9)	17(9)	41(24)
Met N - C4' PLP	2.2-4.3	5.1(5)	5.9(12)		
Met N - NZ K211	2.8-4.6	4.6(6)	5.7(12)		
Met N - O3 PLP	3.1-5.4	6.6(6)	4.0(16)		
Met N - PO_3 PLP	4.3-6.2	5.2(6)	8.8(9)		
Met N - waters[d]	NA	2	1		
Met CO_2 - R375	2.5-3.9	4.7(12)	2.9(4)		

Distances (Å) unless otherwise noted. Distances to an unspecified atom in a protein residue refer to the hydrogen-bonding heavy atom of the side chain (such as S208-OG; see also Fig. 6). [a]From the PDB structures with a co-bound ion or Met analog. [b]Percentage of A orientation for Schiff base (non-apo PDB structures). [c]Angle (°) between PLP and Y144 rings. [d]Number of waters hydrogen bonding.

Finally, in all available PDB structures, the PLP pyridine ring stacks onto Y114 while its (protonated) N1 atom forms a salt bridge with D186. With N2 and Z2, the stacking was fully maintained, and slightly stronger with N2, with the mean ring distances and angles in Table 4. In contrast, N1 and Z1 led to a weaker stacking and a poorer agreement with

the PDB. The N1-D186 salt bridge was fully maintained with N2, and mostly maintained but weaker with Z2. With Z1 and N1, its occupancies were just 79% and 57%.

Overall, the PLP protonation state has a notable effect on the active site structure. MD structures agreed with the PDB when PLP was in its Z2 and especially N2 states, whereas, Z1 and N1 simulations led to discrepancies. This is consistent with the FEP results above, and confirms that N1, Z1 are weakly-populated and N2 predominant.

Structural consequences of Met binding

We turn now to the Met ligand, its interactions, and its effect on the active site structure. The starting pose was taken from the four PDB models that included Met (PDB codes 3aej, 3eam, 3aen, 3vk3). In those models, the Met backbone N pointed towards its reactive target atom—the PLP C4', with distances of 2.2–4.3 Å, and towards the Lys211 NZ and PLP O3, with distances of 2.8–4.6 Å and 3.1–5.4 Å. The Met side chain pointed towards the active site exit, surrounded by the hydrophobic residues F50*, F58*, I62* and V339. The Met carboxylate interacted with the R375 side chain, 2.9 Å away, similar to the co-bound anions in the PDB (Fig. 4).

This pose was not completely stable during MD. With the weakly-populated N1 and Z1 PLP protonation states, Met was highly mobile in the binding site, even moving out of the pocket during one Z1 simulation. We focus however on the N2 and Z2 states, which are the most populated. In Fig. 6, the starting, PDB-based MD pose is compared to a representative MD structure of the N2 state. With N2, the ligand shifted by about 1.4 Å. Its ammonium stayed close to the PLP C4' and the Schiff base Lys211. The N–NZ distance was below 5.5 Å 95% of the time, with a mean of 4.6±0.6 Å, about 1 Å greater than in the initial pose. The C4' and NZ interactions were weaker with Z2. The N–C4' distance was 5.1±0.5 Å with N2, and 5.9±1.2 Å with Z2, distinctly larger than in the

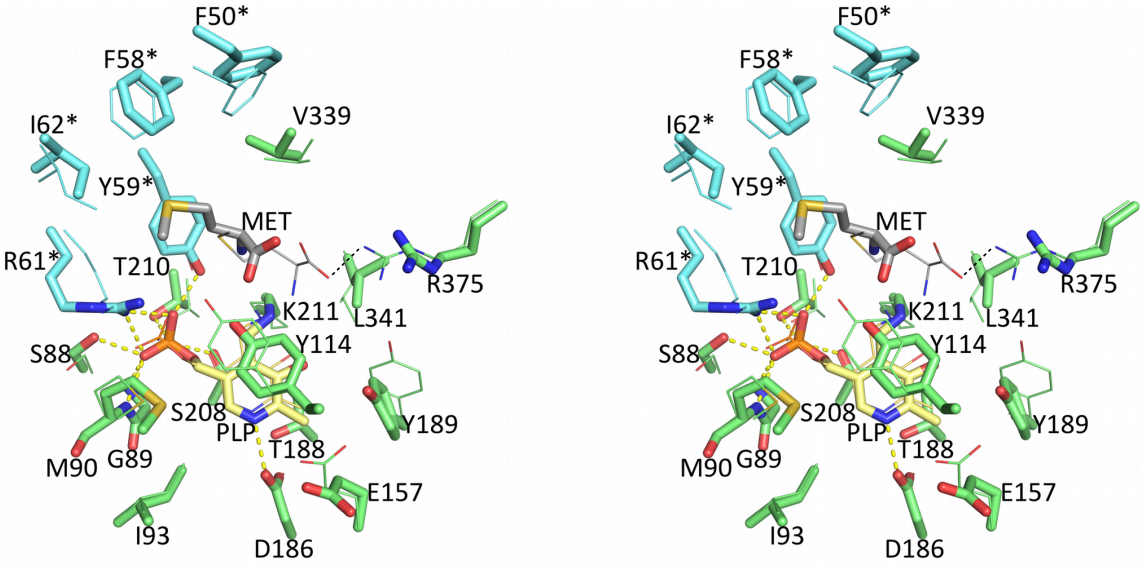

Figure 6: Representative MD structure of Met:MGL-PLP in its N2 protonation state. Cross-eyed stereo view. Met, PLP and selected side chains are shown as sticks. The initial pose is shown as thin lines. Selected interactions are highlighted by dashed lines, including the Met–R375 interaction in the initial pose (thin black dashed line). Residues from an adjacent subunit (light blue) have an asterisk in their labels. Produced with Pymol.

starting pose. With N2, the Met N and the PLP O3 never interacted closely (Fig. 5), whereas they were much closer with Z2, which has an electronegative O3. In its shifted N2 position, the Met ammonium hydrogen bonded only occasionally to Y59* and Y114, but formed a stable interaction with the PLP phosphate through a bridging water, and with a second water. With Z2, Met was more mobile, as shown by its distance fluctuations in Table 4, but it maintained its salt bridge with R375.

From the PDB analysis above, we expected the Met carboxylate to impact the active site structure nearby, shifting the keto/enol equilibrium and the Schiff base orientation. Indeed, the Schiff base always maintained its A orientation with both N2 and Z2, consistent with the PDB structures that have a co-bound anion or carboxylate. In the earlier, apo simulations of Z2 (the dominant apo state), orientation B was seen for the Schiff base 25% of the time.[13] More generally, with bound Met, the active site was more ordered. Phosphate hydrogen bonds were maintained with S208 and T210, the G89 and M90 backbones, and Y59* and R61* from the neighboring subunit. In the apo simulations of Z2, the phosphate interaction with Y59* was broken 20% of the time.[13]

From the FEP calculations above, N2 and Z2 are the most populated PLP protonation states with or without bound Met. However Met binding increases the N2 population 7-fold, from 10% to 69%. This shifts the active site structure from a Z2 to an N2 character, which facilitates the first step of the enzyme reaction. Indeed, N2 Met is in a distinctly better position to react with the PLP C4' and displace NZ (Table 4), thanks to an A orientation for NZ, a moderate N–C4' distance, a Met side chain anchored by four hydrophobic residues, and low fluctuations. Thus, Met helps organize the active site for its own reaction.

Discussion and conclusions

To understand and engineer enzymes, a major difficulty is the unstable character of intermediates along the reaction pathway, which are not amenable to most experimental techniques, including crystallography. The MGL reaction involves several such steps and intermediates (Fig. 1), including the Michaelis complex studied here. A second difficulty is the need to identify the important tautomeric and protonation states in the active site. In particular, protons are not visible in electron density maps. For MGL, the PLP cofactor itself has at least four plausible protonation states. Even the phosphate protonation state and its pK_a are not experimentally known for most PLP enzymes, including MGL.

The molecular modeling used here addresses these difficulties. Our strategy was to model the four main PLP states and derive their occupancies from alchemical free energy perturbation simulations (FEP). Next, we surveyed PDB structures and identified the PLP states that led to the best agreement with PDB data during MD simulations. Each of these steps presents difficulties. PLP force field parameters[13] are imperfect. To interpret the PDB survey, it was important to distinguish structures with and without a co-bound ion or amino acid analog, since apo and non-apo structures displayed subtle but systematic differences. In addition, the Met position had to be modeled, since PDB entries that included Met in their coordinate files did not actually contain electron density for Met. The FEP approach requires extensive MD simulations, and special care when comparing states of the protein that differ in their net charge (eg, due to phosphate protonation). In addition, the relative keto/enol free energies make use of a gas phase reference state treated by quantum mechanics.[13] Finally, computing the phosphate pK_a required a multi-state formalism, derived above in a general form. In contrast, our earlier work used a more approximate method, neglecting the enol/keto free energy difference.

By rigorously computing the free energies of all four PLP protonation states in solution and the protein, with and without bound Met, we showed that the phosphate pK_a in apo-MGL is strongly downshifted compared to solution, so that the fully-deprotonated state is predominant. Met binding modifies the pK_a only slightly, compared to the apo case.

MD simulations yielded structures in good agreement with the PDB data, as long as one focuses on the predominant PLP states and the non-apo MGL structures. The simulations provided additional evidence that Z2 and especially N2 are the predominant PLP protonation states in the Michaelis complex. They also showed that the Met poses found in four PDB models are not very accurate. Rather, MD puts the Met in a shifted position, with somewhat different interactions for its ammonium and carboxylate groups. With the N2 (-2, enol) protonation state, the Met position appears most favorable for the enzyme reaction to proceed. The computed population of this state is increased 7-fold, compared to the apo-enzyme. Thus, Met binding shifts the PLP state towards the one most favorable for the reaction, promoting its own transformation.

We also introduced a simple Michaelis-Menten model (Fig. 1B) to help guide the investigation of various reaction steps and intermediate states and their roles in determining the overall MGL rate. We confirmed experimentally (Table 1) that the reaction is unlikely to bypass the Michaelis complex $\mathcal{M}$, since the covalent PLP linkage is needed for activity. Introducing several approximations that appear at least qualitatively reasonable, we found that the overall rate takes a simple form, proportional to the amount of non-covalently bound PLP. This suggests a further reaction intermediate to focus on in future studies.

The methodology applied here can be used to understand and engineer such reaction intermediates, as well as other MGL enzymes, including the MGL from *Brevibacterium*

aurantiacum. This bacterium is present in food, so that its MGL should be a non-immunogenic candidate for anticancer therapy. Given the high level of homology between its MGL and ppMGL (38% sequence identity), we expect its main structural features, such as the PLP phosphate pK_a, will be similar to those of ppMGL.

Supporting information

Supporting information contains (1) absorbance spectra of wildtype (WT) and mutant MGL proteins, (2) the list of the PDB structures of MGL surveyed in this work, and (3) free energy derivatives from FEP calculations.

Acknowledgements

Support from the Fonds Saint Michel (1 rue Lhuillier 75015 Paris) and the Institut du Cancer et d'Immunogénétique is gratefully acknowledged (ICIG, Hôpital Paul Brousse, 14 ave. Paul Vaillant Couturier, 94807 Villejuif, France). Some of the calculations were run at the CINES supercomputer center of the French Ministry of Education and Research and the TGCC center of the GENCI supercomputing agency.

Accession codes

The Uniprot entry for methionine gamma-lyase from *Pseudomonas putida* is P13254.

References

(1) Sato, D.; Nozaki, T. Methionine gamma-lyase: the unique reaction mechanism, physiological roles, and therapeutic applications against infectious diseases and cancers. *Life* **2009**, *61*, 1019–1028.

(2) Lehninger, A.; Cox, M.; Nelson, D. L. *Principles of Biochemistry*; Freeman, New York, 2008; pp 1736–40.

(3) Schneider, G.; Käck, H.; Lindqvist, Y. The manifold of vitamin B6 dependent enzymes. *Structure* **2000**, *8*, R1–R6.

(4) Eliot, A. C.; Kirsch, J. F. Pyridoxal phosphate enzymes: mechanistic, structural, and evolutionary considerations. *Ann. Rev. Biochem* **2004**, *73*, 383–415.

(5) Machover, D., Rossi, L., Hamelin, J., Desterke, C., Goldschmidt, E., Chadefaux-Vekemans, B., Bonnarme, P., Briozzo, P., Kopecny, D., Pierige, F., Magnani, M., Mollicone, R., Haghighi-Rad, F., Gaston-Mathé, Y., Dairou, J., Boucheix, C. and Saffro, R. Effects in cancer cells of the recombinant L-methionine gamma-lyase from *Brevibacterium auranti-acum.* Encapsulation in human erythrocytes for sustained L-methionine eliminations. *J. Pharma. Exp. Therap.* **2019**, *369*, 489–502.

(6) Lu, W.-C.; Saha, A.; Yan, W.; Garrison, K.; Lamb, C.; Pandey, R.; Irani, S.; Lodi, A.; Lu, X.; Tiziani, S.; Zhang, Y. J.; Georgiou, G.; DiGiovanni, J.; Stone, E. Enzyme-mediated depletion of serum L-Met abrogates prostate cancer growth via multiple mechanisms without evidence of systemic toxicity. *Proc. Natl. Acad. Sci. USA* **2020**, *117*, 13000–11.

(7) Kappes, B.; Tews, I.; Binter, A.; Macheroux, P. PLP-dependent enzymes as potential drug targets for protozoan diseases. *Biochem. Biophys. Acta* **2011**, *1814*, 1567–1576.

(8) Ferreira, G.; Vajapey, U.; Hafez, O.; Hunter, G. A.; Barber, M. J. Aminolevulinate synthase: Lysine 313 is not essential for binding the pyridoxal phosphate cofactor but is essential for catalysis. *Prot. Sci.* **1995**, *4*, 1001–06.

(9) Bertoldi, M.; Cellini, B.; D'Aguanno, S.; Voltattorni, C. B. Lysine 238 is an essential residue for α,β-elimination catalyzed by *Treponema denticola* cystalysin. *J. Biol. Chem.* **2003**, *278*, 37336–43.

(10) Jencks, W. P. *Catalysis in chemistry and enzymology*; Dover, New York, 1986.

(11) Lin, Y.-L.; Gao, J. Internal proton transfer in the external pyridoxal 5'-phosphate Schiff base in dopa decarboxylase. *Biochemistry* **2010**, *49*, 84–94.

(12) Lin, Y.-L.; Gao, J.; Rubinstein, A.; Major, D. T. Molecular dynamics simulations of the intramolecular proton transfer and carbanion stabilization in the pyridoxal 5'-phosphate dependent enzymes L-dopa decarboxylase and alanine racemase. *Biochem. Biophys. Acta* **2011**, *1814*, 1438–1446.

(13) Chen, X.; Briozzo, P.; Machover, D.; Simonson, T. A computational model for the PLP-dependent enzyme methionine γ-lyase. *Front. Molec. Sci.* **2022**, *9*, 886358.

(14) Limbach, H.-H.; Chan-Huot, M.; Sharif, S.; Tolstoy, P. M.; Shenderovich, I. G.; Denisov, G. S.; Toney, M. D. Critical hydrogen bonds and protonation states of pyridoxal 5'-phosphate revealed by NMR. *Biochem. Biophys. Acta* **2011**, *1814*, 1426–1437.

(15) Bennett, C. H. Efficient estimation of free energy differences from Monte Carlo data. *J. Comp. Phys.* **1976**, *22*, 245–268.

(16) Simonson, T. In *Computational Biochemistry & Biophysics*; Becker, O., MacKerell Jr., A. D., Roux, B., Watanabe, M., Eds.; Marcel Dekker, N.Y., 2001; Chapter 9.

(17) Kastenholz, M. A.; Hünenberger, P. H. Computation of methodology-independent ionic solvation free energies from molecular simulations. I. The electrostatic potential in molecular liquids. *J. Chem. Phys.* **2006**, *124*, 224501.

(18) Lin, Y. L.; Aleksandrov, A.; Simonson, T.; Roux, B. An overview of electrostatic free energy computations for solutions and proteins. *J. Chem. Theory Comput.* **2014**, *10*, 2690–2709.

(19) Aksimentiev, A.; Schulten, K. Imaging alpha-hemolysin with molecular dynamics: ionic conductance, osmotic permeability, and the electrostatic potential map. *Biophys. J.* **2005**, *88*, 3745–3761.

(20) Maier, J. A.; Martinez, C.; Kasavajhala, K.; Wickstrom, L.; Hauser, K. E.; Simmerling, C. Improving the accuracy of protein side chain and backbone parameters from ff99SB. *J. Chem. Theory Comput.* **2015**, *11*, 3696–3713.

(21) Brünger, A. T. X-PLOR *version 3.1, A System for X-ray crystallography and NMR*; Yale University Press, New Haven, 1992.

(22) Jorgensen, W. L.; Chandrasekar, J.; Madura, J.; Impey, R.; Klein, M. Comparison of simple potential functions for simulating liquid water. *J. Chem. Phys.* **1983**, *79*, 926–935.

(23) Darden, T.; York, D.; Pedersen, L. Particle mesh Ewald: an N log(N) method for Ewald sums in large systems. *J. Chem. Phys.* **1993**, *98*, 10089–10092.

(24) Feller, S. E.; Zhang, Y.; Pastor, R. W.; Brooks, B. R. Constant pressure molecular dynamics simulation: the Langevin piston method. *J. Chem. Phys.* **1995**, *103*, 4613–4622.

(25) Martyna, G. J.; Tobias, D. J.; Klein, M. L. Constant pressure molecular dynamics algorithms. *J. Chem. Phys.* **1994**, *101*, 4177–4189.

(26) Esaki, N.; Soda, K. Methionine γ-lyase from *Pseudomonas putida* and *Aeromonas* . *Meth. Enzym.* **1987**, *143*, 459–465.

(27) Hill, M. P.; Carroll, E. C.; D., T. M.; Larsen, D. S. Rapid photodynamics of vitamin B6 coenzyme pyridoxal 5'-phosphate and its Schiff bases in solution. *J. Phys. Chem. B* **2008**, *112*, 5867–5873.

(28) Futaki, S.; Ueno, H.; Martínez-del Pozo, A.; Pospischil, M.; Manning, J.; Ringe, D.; Stoddard, B.; Tanizawa, K.; Yoshimura, T.; Soda, K. Substitution of glutamine for lysine at the pyridoxal phosphate binding site of bacterial D-amino acid transaminase. Effects of exogenous amines on the slow formation of intermediates. *J. Biol. Chem.* **1990**, *265*, 22306–22312.

(29) Ziak, M.; Jager, J.; Malashkevich, V. N.; Gehring, H.; Jaussi, R.; Jansonius, J. N.; Christen, P. Mutant aspartate aminotransferase (K258H) without pyridoxal-5'-phosphate-binding lysine residue. Structural and catalytic properties. *Eur. J. Biochem.* **1993**, *211*, 475–484.

Table of contents graphic